

Range-Doppler-Acceleration Estimation for Fast-Moving and Accelerating Targets

Nadav Neuberger, Simon Kollecker, Martin Käske

Abstract—A central aspect of every pulsed radar signal processor is the target’s Range-Doppler estimation within a Coherent Processing Interval. Conventional methods typically rely on simplifying assumptions, such as linear target motion, narrowband operation, or constant velocity, to enable fast computation. However, these assumptions break down in scenarios involving quadratic range-time behavior, high radial velocities or accelerations, or wideband signals, leading to undesired effects such as intra-pulse Doppler shift/stretch and target migration across Range-Doppler cells. This paper presents a generalized waveform-independent Range-Doppler compression approach that compensates for these effects while maintaining minimal Signal-to-Noise-Ratio loss and practical computational efficiency. The performance limits of the proposed method are analyzed and expressed through a unified metric that depends on both scene and system parameters. Comparison with other approaches is presented, showing their estimation bias and performance degradation.

Index Terms—Range-Doppler Compression, High velocity, Supersonic, Quadratic motion, Wideband

I. INTRODUCTION

In radar Signal Processing (SP), the handling of fast-moving or accelerating objects is of central importance. The received echo from a moving target is not only delayed relative to the transmitted waveform but also distorted by Doppler effects, including frequency shifts and time scaling. When multiple pulses are coherently integrated within a Coherent Processing Interval (CPI), these motion-induced effects lead to range and/or Doppler cell migration, thereby degrading the output Signal-to-Noise-Ratio (SNR) and the accuracy of parameter estimation, if not properly taken into account in the processing.

The severity of these distortions depends jointly on the target’s kinematic behavior (e.g., speed, acceleration, and degree of motion non-linearity) and on system parameters such as bandwidth and CPI duration. Three practical regimes can be distinguished. (1) *Slow motion*: The target remains within a single range cell and the radial motion can be treated as approximately constant across the CPI. Standard two-dimensional Fast Fourier Transform (FFT) processing is therefore sufficient [1]. (2) *Linear but significant motion*: The motion is still linear over the CPI but large enough to cause range migration. The Keystone Transform (KT) is widely used for compensating this effect through slow-time rescaling [2]. (3) *High and/or non-linear motion*: When the radial velocity is high, the waveform experiences intra-pulse Doppler shifts

Authors’ address: Fraunhofer Institute for High Frequency Physics and Radar Techniques FHR, Wachtberg, 53343, Germany, e-mail: (nadav.neuberger@fhr.fraunhofer.de).

and time stretching; when the range evolution is quadratic, energy spreads across both range and Doppler dimensions. In such cases, 2D-FFT processing and KT become inadequate, since the waveform distortion must be handled on a per-pulse basis [3]. As an example, scenarios of this type arise in Space Situational Awareness (SSA), where satellites may exhibit radial accelerations on the order of 200 m s^{-2} , and in long-pulse or wideband radar systems where intra-pulse Doppler cannot be ignored.

Despite its relevance, the third regime is insufficiently addressed in the existing literature. Direct time-domain matched filtering is computationally prohibitive, while extensions of KT to quadratic motion [4], [5] are most effective only in the special case of zero initial velocity, with residual errors remaining when linear and quadratic components coexist [6], [7]. KT effectively corrects range migration but does not compensate intra-pulse Doppler modulation or wideband quadratic motion, limiting its applicability in case of long-pulse, high-dynamics scenarios.

Most importantly, all these contributions deals strictly with Linear Frequency Modulation (LFM) waveform, which also impose the Range-Doppler (RD) coupling and Doppler ambiguity issues. In [8], this problem is addressed under restrictive scenario conditions. As shown later, without proper treatment, an estimation bias and SNR loss are unavoidable.

This work extends the approach introduced in [9] with four main contributions:

- Unbiased Range-Doppler-Acceleration (RDA) estimation for any waveform, including LFM.
- A generalized RD compression framework that compensates for both inter-pulse acceleration and intra-pulse Doppler-induced time distortion.
- A new approximation *Cruise-and-Go* that linearizes the delay within each pulse while allowing pulse-to-pulse dynamics, enabling FFT-based matched filtering for quadratic motion.
- A unified performance metric that predicts the framework SNR loss and defines the method’s operational limits.
- An analysis of Doppler-ambiguity behavior in long-pulse/high-velocity regimes and recommendations for waveform selection.

The focus is on developing an efficient implementation that minimizes SNR loss due to model mismatch. The method employs pulse-wise FFT processing with minimal assumptions, making it suitable for unknown quadratic radial motion, high velocities, and long pulses. We will approximate the motion as *Cruise-and-Go*—an analog of the well-known *Stop-and-Go*

assumption. The accuracy and resolution of this method stay intact.

The remainder of this paper is organized as follows. Section II introduces the signal model, including the time-delay formulation under quadratic radial motion. Section III reviews the classical RD processing chain and highlights the assumptions that break down for high-velocity or accelerating targets. Section IV presents the proposed method, including the *Cruise-and-Go* approximation and its resulting FFT-based implementation. Section V evaluates and compares the method through simulations. In Section VI we quantify its limitations, and introduce a unified performance metric for predicting correlation loss. Section VII concludes the paper and summarizes the main findings. The Appendix provides an analytical assessment of the approximation error introduced by the *Cruise-and-Go* assumption.

II. SIGNAL MODEL

In this section, we describe a pulsed radar signal model, taking into account both radial velocity and acceleration. We consider a single moving target, within a single CPI, for a single antenna. We denote the following parameters: the single CPI consists of N_p identical pulses. Its Pulse Repetition Interval (PRI) is T_{pr} and CPI as $T_{\text{cp}} = T_{\text{pr}}N_p$. The fast time variable is Δt , while T_m is the slow-time variable, depending on the m -th pulse index $T_m = T_{\text{pr}}(m-1)$, where $0 \leq \Delta t \leq T_{\text{pr}}$. We emphasize that $t \in [t_0, t_0 + T_{\text{cp}}]$ represents the elapsed time since the CPI start. For simplicity, we choose $t_0 = 0$ since we will consider a single CPI throughout the paper.

A. Time-Delay

In some radar applications (e.g. SSA), the potential targets could be thousands of kilometers away, which requires the use of unambiguous long Tx pulses, to allow higher energy transmission. In addition, the radial velocity and acceleration can reach high values (hypersonic), and the Doppler shift can have an impact even within a single pulse.

We start with a single pulse derivation, and extend it later to a train of pulses. In Fig. 1 we illustrate the range of a single target (i.e. distance between Tx/Rx and target) having a quadratic range-profile. Note that the scenario is exaggerated for illustrative purposes especially with respect to the speed-of-light c_0 and thus the time it takes the pulse to intercept the target. We distinguish the following parameters: t is the global timestamp (in seconds), elapsed time since the beginning of the CPI, named t_0 . Let $\tau(t)$ be the two-way delay of a sample transmitted at $t_{tx}(t)$, reflected at t' , and received at time t . This delay depends on the target range at $t' = t - \tau(t)/2$.

The transmission time stamp $t_{tx}(t)$ corresponds to an arbitrary sample of the Tx pulse. For example, for a signal received at time t_5 , we have $t' = t_3$ and $t_{tx}(t_5) = t_1$, and $\tau(t_5) = t_5 - t_1$. The stretching effect is shown due to the high radial velocity, as the received pulse length is longer than the transmitted one. We can now formulate

$$\tau(t) = t - t_{tx}(t) = \frac{2}{c_0} r(t - \tau(t)/2). \quad (1)$$

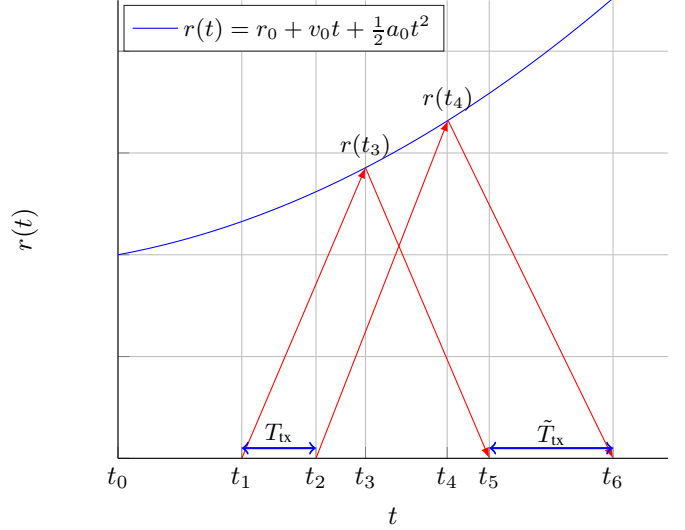


Fig. 1. Delay induced on transmitted signal by a target with quadratic range-profile. Within one pulse, we illustrate two transmitted samples (beginning and end of the waveform) at times t_1, t_2 , and received at times t_5, t_6 respectively. The stretching effect is shown due to the high radial velocity—the received pulse length \tilde{T}_{tx} is longer than T_{tx} .

This accurate implicit expression of the delay is commonly replaced with $\tau(t) = 2r(t)/c_0$, which approximates the range of the target at time of interception as t instead of the accurate value t' .

The down-converted baseband signal echo that arrives to a single antenna at time snapshot t , for a single pulse, caused by a single point target with parameters θ_0 can be expressed as

$$y(t, \theta_0) = A \underbrace{s[t - \tau(t, \theta_0)] e^{-i2\pi f_c \tau(t, \theta_0)}}_{b(t, \theta_0)}. \quad (2)$$

$\tau(t, \theta_0)$ is the fast-time dependent two-way delay of a wave reflected by the target and arriving at the receiver at times t . It depends on the target's parameters vector θ_0 at the initial timestamp of the CPI t_0 . The carrier wave frequency is f_c , and the amplitude A depends on the range (representing the propagation loss), the target's Radar Cross Section (RCS), and antenna Direction of Arrival (DOA) two-way gain. For simplicity and without loss of generality, we will assume it to be unity and ignore any DOA aspects for the remainder of the text.

We will treat the case of a quadratic time-dependent range, where $\theta_0 = [r_0, v_0, a_0]$, with r_0, v_0, a_0 as the initial range, radial velocity and acceleration of the target, respectively. The range follows

$$r(t, \theta_0) = r_0 + v_0 t + \frac{1}{2} a_0 t^2. \quad (3)$$

From (1) and (3), we can now write

$$\frac{c_0}{2} \tau(t) = r_0 + v_0 (t - \tau(t)/2) + \frac{1}{2} a_0 (t - \tau(t)/2)^2. \quad (4)$$

In the next sections we will show two different approaches to approximate $\tau(t)$.

B. Range-Doppler Compression

One central aspect in every radar SP scheme is the RD compression. This crucial and computationally demanding process estimates the RD values of the target, under an assumed motion model. The unknowns in θ_0 are estimated using a correlation (or matched-filter) based approach where the actual received data is correlated with the template signal. The set of parameters maximizing the correlator (absolute) output is used as an estimate of θ_0 . We now write the RD equation of a single pulse, for a specific choice of target's parameters θ_0 , as

$$\begin{aligned} RD(\theta_0) &= \int x(t)b^*(t, \theta_0) dt \\ &= \int x(t)s^*[t - \tau(t, \theta_0)] e^{i2\pi f_c \tau(t, \theta_0)} dt. \end{aligned} \quad (5)$$

where $x(t)$ is the received measured baseband signal, and $b(t, \theta_0)$ is used as the template signal. The SNR is derived from the response magnitude and the known noise statistical distribution. When integrating a series of N_p pulses, the complex (coherent) or magnitude (non-coherent) output of (5) is summed up for all pulses. Its direct time-domain calculation has a heavy computational load, which prevents any practical response time.

III. CLASSICAL METHOD

There are several simplifications and assumptions that can be made to compute (5) using FFT. These are very common, usually permitted by the application scenario and allow a fast and practical computation time. We present this simplified scenario derivation as a theoretical basis and motivation for our proposed method in Section IV.

In the case of a single pulse, where the radial velocity of the target is low such that the motion within the pulse is negligible in terms of range resolution and phase, we can simplify (1) into

$$\tau(t, \theta_0) \approx \frac{2r(t_0, \theta_0)}{c_0} = \frac{2r_0}{c_0} = \tau_0, \quad (6)$$

and re-write (5) as

$$RD(\theta_0) = e^{i2\pi f_c \tau_0} \int x(t)s^*[t - \tau_0] dt. \quad (7)$$

The next step is crucial—transforming the equation into two separate functions, to allow a time-convolution equivalent with an FFT operation. The definition of a convolution is

$$(u(t) \circledast v(t))(\alpha) = \int u(t)v(\alpha - t)dt. \quad (8)$$

We denote two auxiliary functions

$$\begin{aligned} u(t) &= x(t) \\ v(t) &= s^*(-t) \end{aligned}$$

such that

$$RD(\tau_0) = e^{i2\pi f_c \tau_0} (u(t) \circledast v(t)) \Big|_{\alpha=\tau_0}. \quad (9)$$

The complex output value represents the magnitude and phase of the target echo. Since time-convolution is equivalent to multiplication in the Fourier domain, we can write

$$RD(\tau_0) = e^{i2\pi f_c \tau_0} \mathcal{F}^{-1}\{X(f)V(f)\} \Big|_{t=\tau_0}, \quad (10)$$

where $X(f) = \mathcal{F}(u(t))$, $V(f) = \mathcal{F}(v(t))$, and \mathcal{F} is the FFT operator. This step is the so-called 1D *Range Compression* which is done as a first stage in the SP sequence. We note that $V(f)$ can be pre-calculated once ('offline'), leaving only the calculation of $X(f)$ in real-time. For a pre-defined set of values of τ_0 , we choose the maximum absolute value for (10) as the estimate of the target's delay (or range)

$$\hat{\tau}_0 = \operatorname{argmax}_{\tau_0} |RD(\tau_0)|. \quad (11)$$

When integrating multiple pulses, the *stop-and-go* approximation is widely used. It assumes the target does not move during the transmission of a single pulse; its location only updates once between one pulse and the next one. Hence, the RD output of each pulse will depend on the pulse index.

With the assumption of a constant radial velocity throughout the CPI, the two-way target delay at the start of the m -th pulse is

$$\tau_m = \tau_0 + \frac{2v_0 T_m}{c_0}, \quad (12)$$

where the '0' subscript points to the beginning of the CPI. The *stop-and-go* assumption states that $\tau(t) = \tau_m$ for $T_m < t < T_{m+1}$. By plugging this expression in (5) we get

$$\begin{aligned} RD_m(\tau_0, v_0) &= \\ &e^{i2\pi f_c \frac{2v_0 T_m}{c_0}} e^{i2\pi f_c \tau_0} \int x_m(t)s^* \left[t - \tau_0 - \frac{2v_0 T_m}{c_0} \right] dt. \end{aligned} \quad (13)$$

By disregarding any range migration due to the low velocity, poor range resolution, or short CPI, we reach the coherent integration expression

$$\begin{aligned} RD(\tau_0, v_0) &= \\ &e^{i2\pi f_c \tau_0} \sum_{m=1}^{N_p} e^{i2\pi f_c \frac{2v_0 T_m}{c_0}} \int x_m(t)s^* [t - \tau_0] dt. \end{aligned} \quad (14)$$

This could be seen as a two-step process, the first the complex output FFT range compression given by (10), followed by another Inverse Fast Fourier Transform (IFFT) over slow-time with the Doppler frequency shift $f_d = -2v_0 f_c / c_0$. Taking the magnitude gives

$$\begin{aligned} |RD(\tau_0, v_0)| &= \\ &\left| \mathcal{F}_{\text{st}}^{-1} \left\{ \mathcal{F}_{\text{ft}}^{-1} \{ X_m(f)V(f) \} \Big|_{t=\tau_0} \right\} \Big|_{f=f_d} \right|, \end{aligned} \quad (15)$$

where the subscripts *st* and *ft* mean slow time and fast time inverse Fourier transform. The values of τ_0, v_0 that maximize (15) are the RD estimations. Using two sequential IFFTs provide a fast output, and as we see next, cannot be used when some of the simplifications above are prohibited. However, the notion of exploiting FFT is the main drive for the proposed method.

IV. PROPOSED RDA ESTIMATION METHOD

While the classical method is fast and practical, it fails to deal with a non-negligible radial acceleration and Doppler shift/stretch within a single pulse. The motivation in this section, is therefore to present a new RD compression method that

- 1) Compensates radial acceleration from pulse to pulse, both in phase and in range and radial velocity migration and
- 2) Compensates radial velocity even within a single pulse (i.e. no *stop-and-go* approximation) in both Doppler frequency shift and intra-pulse range migration.

We will be able to realize it via a single approximation and the resulting method is still suitable for fast time FFT.

A. Cruise and Go

While the true motion is quadratic, the velocity change within a single pulse is usually small compared to its change across the CPI. Therefore, we approximate the velocity within each pulse as constant, but allow it to vary per pulse. This linearizes the delay $\tau(t)$ with respect to Δt , enabling matched filtering via standard FFT operations with only frequency remapping. We coin the term *Cruise* for constant-velocity motion and *go* when acceleration resumes.

The time t is formalized as a sum of fast and slow time terms, $t = T_m + \Delta t$. We denote $s(t)$ as the transmitted baseband signal (a single pulse with duration T_p) as $s(t) = s(T_m + \Delta t) = s_m(\Delta t) = s(\Delta t)$. The range and radial velocity at the beginning of the m -th pulse are (see Eq. (3))

$$\begin{aligned} v_m &= v_0 + a_0 T_m \\ r_m &= r_0 + v_0 T_m + \frac{1}{2} a_0 T_m^2. \end{aligned} \quad (16)$$

We now explicitly write the *Cruise-and-Go* assumption, where the radial velocity within each pulse is constant (i.e. $a_m = 0$) such that

$$\begin{aligned} v(T_m < t < T_{m+1}) &= v_m \\ r(T_m < t < T_{m+1}) &= r_m + v_m \Delta t. \end{aligned} \quad (17)$$

B. Mathematical Derivation

Solving (1) will now give

$$\tau(t) = \frac{2}{c_0} r(t - \tau(t)/2) = \frac{2}{c_0} \left(r_m + v_m \cdot (\Delta t - \tau(t)/2) \right),$$

which yields

$$\begin{aligned} \tau(t) &= \phi_m + \gamma_m \Delta t, \\ \phi_m &= \frac{2r_m}{c_0 + v_m}, \quad \gamma_m = \frac{2v_m}{c_0 + v_m}. \end{aligned} \quad (18)$$

The parameter γ_m describes the intra-pulse Doppler-induced time scaling. Going back to the RDA expression, we plug (18) into (5) and derive the m -th pulse RDA output as

$$\begin{aligned} RDA_m(\theta_0) &= \int x_m(\Delta t) s^* [\Delta t - \tau(t)] e^{i2\pi f_c \tau(t)} d\Delta t \\ &= e^{i2\pi f_c \phi_m} \int x_m(\Delta t) s^* [(1 - \gamma_m) \Delta t - \phi_m] e^{i2\pi f_c \gamma_m \Delta t} d\Delta t \\ &= e^{i2\pi f_c \alpha} \int x_m(\Delta t) s^* [-(1 - \gamma_m)(\alpha - \Delta t)] \\ &\quad \times e^{-i2\pi f_c \gamma_m (\alpha - \Delta t)} d\Delta t, \end{aligned} \quad (19)$$

with $\alpha = \phi_m / (1 - \gamma_m) = 2r_m / (c_0 - v_m)$.

Following the convolution-based formulation used in Section III, we choose two auxiliary functions

$$\begin{aligned} u_m(t, \gamma_m) &= x_m(t) \\ v_m(t, \gamma_m) &= s^*(-(1 - \gamma_m)t) e^{-i2\pi f_c \gamma_m t}, \end{aligned}$$

such that

$$\begin{aligned} RDA_m(\theta_0) &= e^{i2\pi f_c \alpha} (u_m(t) \circledast v(t, \gamma_m))(\alpha). \end{aligned} \quad (20)$$

In the Fourier domain it calculates as

$$\begin{aligned} RDA_m(\theta_0) &= \frac{1}{|1 - \gamma_m|} e^{i2\pi f_c \alpha} \\ &\quad \times \mathcal{F}^{-1} \left\{ X_m(f) S^* \left(\frac{f + f_c \gamma_m}{1 - \gamma_m} \right) \right\}^\alpha. \end{aligned} \quad (21)$$

The IFFT output is sampled at the timestamps given by

$$\begin{aligned} \alpha &= \frac{\phi_m}{1 - \gamma_m} = \frac{2r_m}{(c_0 + v_m)(1 - \gamma_m)} \\ &= \frac{2r_0}{c_0 - v_m} + \zeta_m, \end{aligned}$$

where $\zeta_m = 2(v_0 T_m + 0.5 a_0 T_m^2) / (c_0 - v_m)$. This expresses the sampling location in terms of scaled delay plus a motion-induced offset ζ_m . In the Fourier domain it writes

$$\begin{aligned} RDA_m(\theta_0) &= \frac{1}{|1 - \gamma_m|} e^{i2\pi f_c \alpha} \\ &\quad \times \mathcal{F}^{-1} \left\{ X_m(f) S^* \left(\frac{f + f_c \gamma_m}{1 - \gamma_m} \right) e^{i2\pi f \zeta_m} \right\} \Big|_{\hat{\alpha} = \frac{2r_0}{c_0 - v_m}}. \end{aligned} \quad (22)$$

We now introduce the auxiliary parameter $\rho_m = (c_0 - v_m) / c_0$ which represent the required frequency-domain scaling. Together with the effective sampling location $\hat{\alpha}$ and ζ_m , these allow the RDA output to be evaluated on a uniform delay grid without time-domain interpolation. The output is now sampled at the final desired delay points $\tau_0 = 2r_0 / c_0$:

$$\begin{aligned} RDA_m(\theta_0) &= \frac{\rho_m}{|1 - \gamma_m|} e^{i2\pi f_c \alpha} \\ &\quad \times \mathcal{F}^{-1} \left\{ X_m(\rho_m f) S^* \left(\rho_m \frac{f + f_c \gamma_m}{1 - \gamma_m} \right) e^{i2\pi \rho_m f \zeta_m} \right\} \Big|_{\hat{\alpha} = \tau_0}. \end{aligned} \quad (23)$$

This way, we can pre-compute $S(f)$ and $X(f)$ with a large up-sampling factor, and then interpolate to get the exact value.

The coherent integration across all pulses will therefore yield

$$RDA(\boldsymbol{\theta}_0) = \left| \sum_{m=1}^{N_p} RDA_m(\boldsymbol{\theta}_0) \right|. \quad (24)$$

For every combination of v_0 and a_0 , this sum is computed, and the set $[r_0, v_0, a_0]$ that maximize $RDA(\boldsymbol{\theta}_0)$ is chosen. Due to the pulse-dependent Doppler scaling and delay offsets introduced by acceleration, there is no apparent way to perform a second step of slow-time FFT. Therefore, only pulse-wise FFT was achieved for this scenario, which enables practical computation time, reducing it from $\mathcal{O}(N_p N_r N_t)$ to $\mathcal{O}(N_p(N_r + 2N_t) \log(N_r + 2N_t))$ per v_r and a_r cell, where N_p is the number of pulses, N_r is the number of range samples and N_t is the number of samples of the transmission pulse. The speedup is

$$\frac{N_r N_t}{(N_r + 2N_t) \log(N_r + 2N_t)}. \quad (25)$$

It considers quadratic range behavior, range and Doppler migration, waveform stretch/compression.

V. PERFORMANCE COMPARISON

In this section, we present three main sections that simulate scenarios where

- Radial acceleration needs to be compensated from pulse to pulse
- The target migrates in range cells during the pulse length and the wave's traveling time (intrpulse range migration or stretch)
- Only a Doppler-intolerant (i.e. not an LFM) waveform allows ambiguity resolution

While the first point has been seen in the literature several times, the authors are not aware of any literature that compensates for the second point. The third example shows a fundamental drawback of methods restricted to LFM, such as [8].

A. Inter-Pulse Acceleration Compensation

As a basic motivation, we start with an example consisting of a long CPI, where compensation of radial acceleration is necessary to achieve a focused peak. We consider a scenario that induces pronounced nonlinear RD migration. The simulation parameters are summarized in Table I. We intentionally use a Costas waveform to isolate motion-induced distortions from waveform-induced RD coupling, enabling a clean evaluation of the processing method.

Fig. 2 shows two RD maps of a target with an initial radial velocity of 500 m s^{-1} and a radial acceleration of 300 m s^{-2} , processed according to (24). These scenarios are representative of spaceborne objects and hypersonic airborne platforms. In the top panel, the data are processed under the incorrect assumption of zero acceleration ($a_0 = 0$). The resulting response is severely defocused—mainly along

TABLE I
SIMULATION PARAMETERS

Symb.	Parameter	Value
f_c	transmit frequency	1.3 GHz
B	bandwidth	8 MHz
T_{pr}	pulse rep. interval	5 ms
T_p	pulse length	2 ms
r_0	range of target	310 km
v_0	rad. vel. of target	500 m s^{-1}
a_0	rad. acc. of target	300 m s^{-2}
N_p	no. of pulses	120

the Doppler dimension—because the target velocity increases from 500 m s^{-1} to approximately 680 m s^{-1} over the 0.6 s CPI. This velocity change spreads the target energy across many Doppler bins and reduces the peak SNR by nearly 20 dB. Moreover, the defocusing follows a curved trajectory rather than a vertical ridge, which prevents coherent integration of energy from a single range cell, or any de-chirping methods.

The bottom plot shows the result when the correct ac-

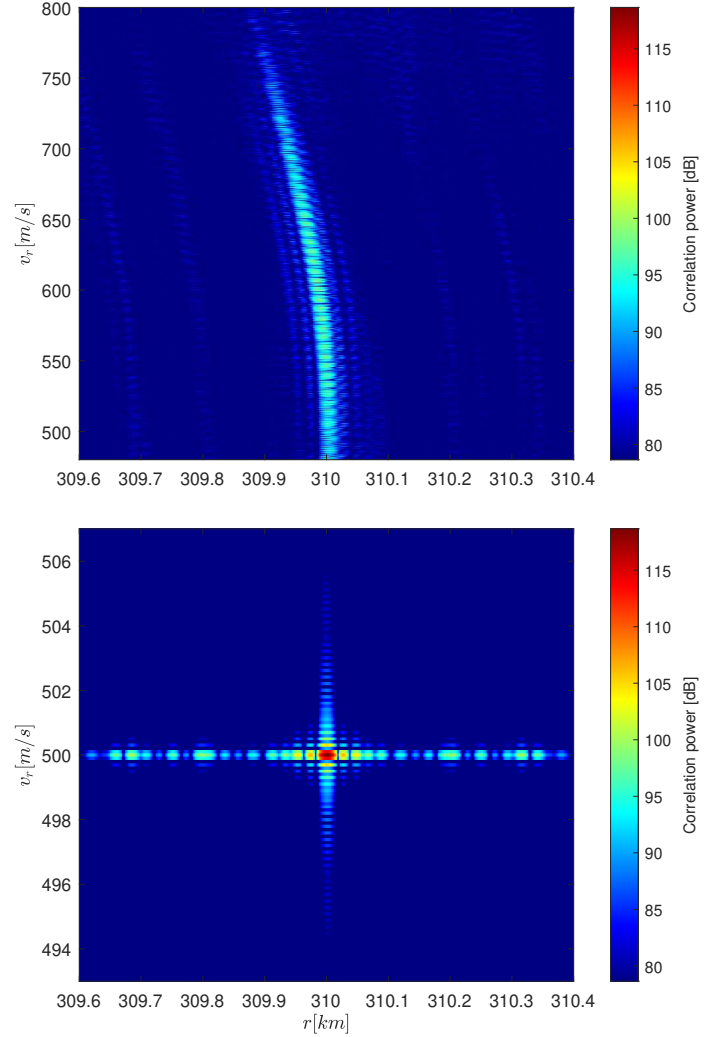


Fig. 2. RD maps with and without acceleration compensation. The corresponding parameters are listed in Table I. The method is compensating for $a_0 = 0$ in the top plot and for the correct $a_0 = 300 \text{ m s}^{-2}$ in the bottom plot.

celeration ($a_0 = 300 \text{ m s}^{-2}$) is applied. Here, the energy is sharply focused in both range and Doppler, confirming that acceleration compensation is essential for long CPIs involving targets with significant radial dynamics. This example primarily illustrates the need for *inter-pulse* acceleration compensation.

B. Stretch for Intra-Pulse Range Migration

This aspect of comparison will illustrate the need for pulse-wise stretch compensation. When pulses are long and radial velocity is high, the frequently used *stop-and-go* approximation is no longer valid. This comparison applies for any method that is not incorporating pulse-wise compensation. In Table II we show the simulation parameters used to emphasize this effect.

TABLE II
SIMULATION PARAMETERS

Symb.	Parameter	Value
f_c	transmit frequency	2 GHz
B	bandwidth	80 MHz
T_{pr}	pulse rep. interval	30 ms
T_p	pulse length	6 ms
r_0	range of target	1000 km
v_0	rad. vel. of target	4 m s^{-1}
a_0	rad. acc. of target	0 m s^{-2}
N_p	no. of pulses	5

Fig. 3 shows the proposed method, with and without pulse-wise stretch compensation. In red, the factor $1 - \gamma_m$ in (19) was used. We see an SNR degradation of 15 [dB] and a worst case range bias of 50 meters (which spans over multiple range cells).

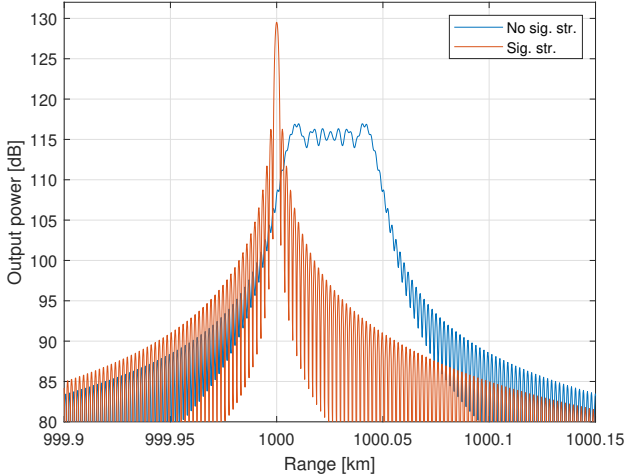


Fig. 3. Correlation of a simulated noise free target with the proposed method without (blue) and with (red) signal stretch (intra-pulse range migration). The waveform is a chirp and the target and system parameters are given in Table II.

C. Doppler Ambiguity Considerations

In the scenarios considered throughout the paper, the radial velocity usually exceeds the unambiguous Doppler interval

TABLE III
SIMULATION PARAMETERS

Symb.	Parameter	Value
f_c	transmit frequency	1.3 GHz
B	bandwidth	2 MHz
T_{pr}	pulse rep. interval	27 ms
T_p	pulse length	4.5 ms
r_0	range of target	1000 km
v_0	rad. vel. of target	0 m s^{-1}
a_0	rad. acc. of target	0 m s^{-2}
N_p	no. of pulses	6

defined by the Pulse Repetition Frequency (PRF), and the resulting ambiguities must therefore be resolved. It should be emphasized that these ambiguities do not originate from any processing method, but arise naturally in the these scenarios. Several primary methods exist for resolving them, provided the radar parameters allow it.

One approach relies on range migration, which can resolve Doppler ambiguities when both the CPI and signal bandwidth are sufficiently large, e.g. [8]. The second approach is single-pulse Doppler processing, which requires a high duty cycle, adequate target SNR, and a Doppler-intolerant waveform. A third solution could be the use of staggered PRI, at the cost of dynamic range. To illustrate the issue and its solution using the second approach, Fig. 4 shows the simulation of the parameters described in Table III.

The RD maps are computed with our method for a noise-free, stationary target. The first example uses a LFM waveform (Doppler-tolerant), while the second one uses a Costas code (Doppler-intolerant), both with a duty cycle of approximately 16 %. In this example, the low bandwidth and PRF, as well as the short CPI prevent the use of range migration for radial velocity ambiguity resolution. Since the PRF is constant, single pulse Doppler is the only remaining option.

In the LFM case, the output is inherently ambiguous, and the RD coupling is clearly visible: a shift in radial velocity can be compensated by a corresponding shift in range. In contrast, the Costas code produces only a few significant ambiguity sidelobes near the true peak, and only the correct Doppler bin attains full coherent gain. In this case, a sufficiently strong SNR is required. The maxima of the first 4 ambiguities have an SNR of -0.41 , -1.7 , -4 and -7.9 dB relative to the main peak. Those values mainly depend on the dutycycle T_p/T_{pr} of the system, where a higher dutycycle corresponds to higher dynamic difference between the main lobe and the ambiguity sidelobes. The issues with the LFM waveform presented here are universal for all methods that use LFM and are a direct drawback of the range-Doppler coupling that is exploited in [8].

D. Comparison Summary

In summary, classical RD processing and KT-based approaches rely on assumptions of negligible intra-pulse Doppler, linear motion, or waveform-specific structure (typically LFM). In the high-velocity, long-pulse, and accelerating scenarios considered here, these assumptions are violated, leading to RD defocusing, estimation bias, or significant SNR

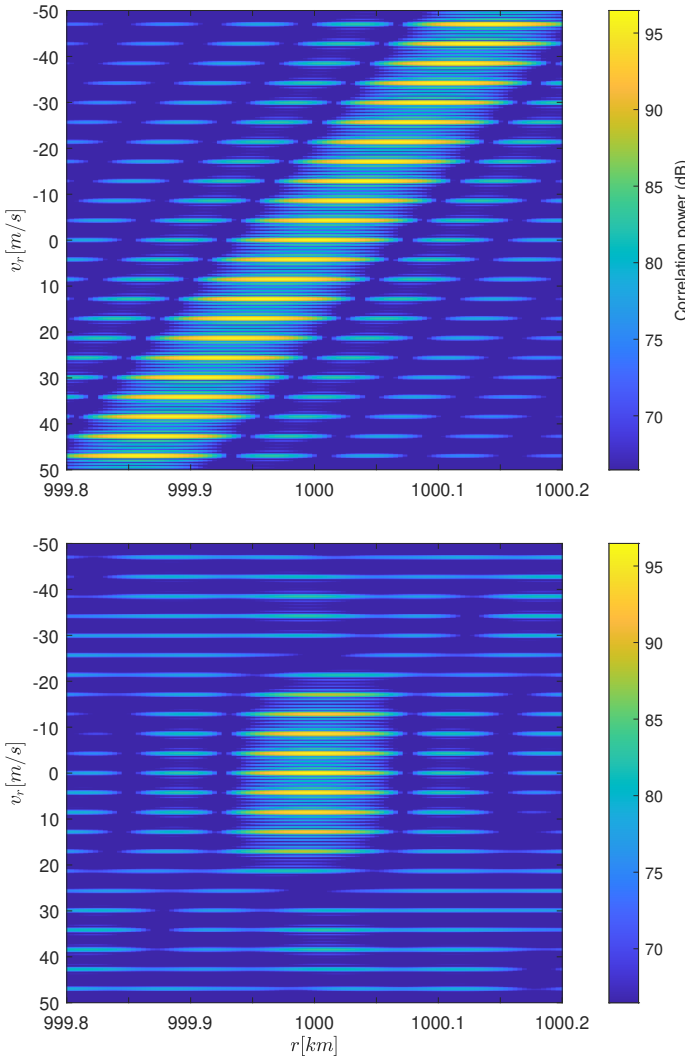


Fig. 4. RD maps with LFM (top) and Costas (bottom) waveform for a simulated target. The target and system parameters are given in Table III.

loss. The proposed method explicitly compensates both inter-pulse acceleration and intra-pulse Doppler-induced distortion in a waveform-independent manner, enabling real-time practical, unbiased RDA estimation under conditions where existing methods are either inaccurate or not applicable.

VI. METHOD GENERALIZATION

An analysis of the limitations of the proposed method is presented, in order to quantify for which systems/scenarios it is suitable. The residual error arises from uncorrected quadratic motion within each pulse. As a result, under conditions of high radial acceleration and long pulse durations, the method may still exhibit performance degradation.

To analyze the possible residual error of the *Cruise-and-Go* assumption, a noise-free target was simulated across a wide range of parameter combinations, listed in Table IV. For all those 1664 parameter combinations listed there, (24) was computed and compared with the theoretical accurate value from (5). We refer to the ratio between them as the correlation loss, expressed in decibels. It was empirically found that this

TABLE IV
GENERAL SIMULATION PARAMETERS

Symb.	Parameter	Value
f_c	transmit frequency	650 MHz, 1300 MHz
B	bandwidth	2 MHz
T_{pr}	pulse rep. interval	25 ms, 50 ms, 75 ms, 100 ms
T_p	pulse length	4 ms, 8 ms
r_0	range of target	3000 km, 10 000 km
v_0	rad. vel. of target	0, 4000 m s ⁻¹
a_0	rad. acc. of target	0, 50 m s ⁻² , ..., 600 m s ⁻²
N_p	no. of pulses	12, 24

loss can be accurately predicted using a specific dimensionless ratio that depends on both system and scene parameters. The so-called *acceleration ratio* is

$$\Upsilon = a T_p (T_p + \tau) / \lambda_c. \quad (26)$$

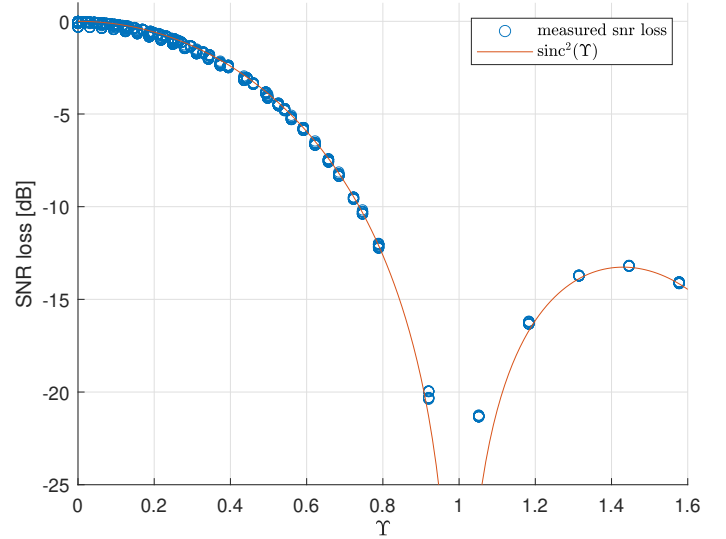


Fig. 5. SNR loss of proposed method in dependence on acceleration ratio. In every case, a target was simulated and processed at the correct v_0 and a_0 and r_0 . The resulting power, divided by the theoretical power of a perfect signal compensation, was plotted here, against the acceleration ratio. The parameter combinations used are given in Table IV.

Fig. 5 shows the observed correlation loss as a function of Υ , alongside the sinc^2 function for comparison. The close alignment of nearly all data points with the sinc^2 curve—despite the wide range of parameter variations—suggests that this function serves as a reliable estimator of the correlation loss.

We now have a tool for the radar system designer, with a quick way to estimate the method's performance. While a, τ are scene related (targets' radial acceleration and range), the radar designer can properly choose T_p, λ_c .

VII. CONCLUSIONS

In contrast to classical RD and KT-based approaches, we have presented a novel method that implements

- 1) Compensation of radial acceleration from pulse to pulse, both in phase and in range and radial velocity migration

- 2) Compensation of radial velocity even within a single pulse (i.e. no stop-and-go approximation) in both Doppler frequency shift and intrapulse range migration
- 3) Flexibility to choose an arbitrary waveform (not restricted to LFM)

The first capability is primarily required for long CPIs and high accelerations, while the second point is required for long pulses and high radial velocities. Although often neglected, in certain scenarios these aspects can be critical, and may experience significant performance degradation without a practical, real-time compensation method and minimal SNR loss.

The special Doppler ambiguity phenomena that these scenarios involve are presented along with several possible solutions. The accuracy and limitation of the approach are presented. We provided an empirically-based predictive metric to guide system design.

APPENDIX

APPROXIMATIONS ANALYSIS

Presented here is a theoretical analysis of the assumption made in the new approach. It provides a sufficient condition for when the assumption is justified. The goal is to quantify the corresponding inaccuracies as a function of target and system parameters.

For $t \in [0, T_{\text{cp}}]$, let $r_{\max} = \max_t r(t)$, $\tau_{\max} = \max_t \tau(t)$ and $v_{\max} = \max_t |\dot{r}(t)|$. Note the absolute value in the definition of v_{\max} . The only approximation made here is the linearization of the motion inside the single pulse. The general formula of the delay is (1), whereas the linearized version is (18), so we are trying to justify

$$2 \frac{r(t - \tau(t)/2)}{c_0} \approx \frac{2r_m + 2v_m \Delta t}{c_0 + v_m}. \quad (27)$$

To this end, let us define the terms

$$\begin{aligned} \varepsilon_1(t) &= \frac{a_0 \tau^2(t)}{4(c_0 + v_0 + a_0 t)} \\ \varepsilon_2(t) &= -\frac{a_0 \Delta t (2r_0 + 2v_0 t + a_0 t^2)}{(c_0 + v_0 + a_0 T_m)(c_0 + v_0 + a_0 t)} \\ \varepsilon_3(t) &= -\frac{a_0 \Delta t^2}{c_0 + v_0 + a_0 t} \\ \varepsilon_{\Sigma}(t) &= \varepsilon_1(t) + \varepsilon_2(t) + \varepsilon_3(t). \end{aligned}$$

These are the neglected terms, because

$$\begin{aligned} \tau(t, \theta_0) &= \frac{2r \left(t - \frac{\tau(t)}{2} \right)}{c_0} \\ &= \frac{2r_0 + 2v_0 t + a_0 t^2 + \frac{1}{4} a_0 \tau^2(t)}{c_0 + v_0 + a_0 t} \\ &= \frac{2r_0 + 2v_0 t + a_0 t^2 - a_0 \Delta t^2}{c_0 + v_0 + a_0 T_m} + \varepsilon_1(t) + \varepsilon_2(t) + \varepsilon_3(t) \\ &= \frac{2r_0 + 2v_0 T_m + a_0 T_m^2 + 2v_0 \Delta t + 2a_0 T_m \Delta t}{c_0 + v_0 + a_0 T_m} + \varepsilon_{\Sigma}(t) \\ &= \frac{2r_m + 2v_m \Delta t}{c_0 + v_m} + \varepsilon_{\Sigma}(t), \end{aligned}$$

where the fourth equality comes from the fact that

$$\frac{a}{b + \varepsilon} = \frac{a}{b} - \frac{a\varepsilon}{b(b + \varepsilon)}. \quad (28)$$

In order to limit ε values we observe that $0 \leq \Delta t \leq T_p + \tau_{\max}$ is the time interval used in the computation. Therefore, the errors are bound by

$$\begin{aligned} |\varepsilon_1(t)| &\leq \frac{|a_0| \tau_{\max}^2}{4(c_0 - v_{\max})} \\ |\varepsilon_2(t)| &\leq \frac{|a_0| (T_p + \tau_{\max}) r_{\max}}{(c_0 - v_{\max})^2} \\ |\varepsilon_3(t)| &\leq \frac{|a_0| (T_p + \tau_{\max})^2}{(c_0 - v_{\max})^2}. \end{aligned}$$

Hence, a sufficient condition is that all of the terms above are significantly lower than $1/f_c$.

REFERENCES

- [1] M. Richards, *Fundamentals Of Radar Signal Processing*. McGraw-Hill, 2005.
- [2] R. Perry, R. DiPietro, and R. Fante, "SAR imaging of moving targets," *IEEE Transactions on Aerospace and Electronic Systems*, vol. 35, no. 1, pp. 188–200, 1999.
- [3] M. Döbereiner, M. Käské, A. Schwind, C. Andrich, M. A. Hein, R. S. Thomä, and G. D. Galdo, "Joint high-resolution delay-doppler estimation for bi-static radar measurements," in *2019 16th European Radar Conference (EuRAD)*, 2019, pp. 145–148.
- [4] D. Kirkland, "Imaging moving targets using the second-order keystone transform," *Radar, Sonar and Navigation, IET*, vol. 5, pp. 902 – 910, 11 2011.
- [5] "An alternative range migration correction algorithm for focusing moving targets," *Progress In Electromagnetics Research*, vol. 131, pp. 227–241, 2012.
- [6] K. M. Scott, W. C. Barott, and B. Himed, "The keystone transform: Practical limits and extension to second order corrections," in *2015 IEEE Radar Conference (RadarCon)*, 2015, pp. 1264–1269.
- [7] A. Filip-Dhaubadel and D. Shutin, "Long coherent integration in passive radar systems using super-resolution sparse bayesian learning," *IEEE Transactions on Aerospace and Electronic Systems*, vol. 57, no. 1, pp. 554–572, 2021.
- [8] B. Hennessy, D. A. Holdsworth, H. Yardley, R. Debnam, G. Warne, and M. Jessop, "Effects of range doppler-rate coupling on high frequency chirp radar for accelerating targets," in *2023 IEEE International Radar Conference (RADAR)*, 2023, pp. 1–6.
- [9] H. Wilden, N. Ben Bekhti, R. Hoffmann, C. Kirchner, R. Kohlleppel, C. Reising, A. Brenner, and T. Eversberg, "GESTRA - recent progress, mode design and signal processing," in *2019 IEEE International Symposium on Phased Array System Technology (PAST)*, 2019, pp. 1–8.